Journal of Alloys and Compounds 509 (2011) 982–989

Contents lists available at ScienceDirect

Journal of Alloys and Compounds

journal homepage: www.elsevier.com/locate/jallcom

Microstructure and mechanical properties of laser welded dissimilar DP600/DP980 dual-phase steel joints

N. Farabi [a], D.L. Chen [a,*], Y. Zhou [b]

[a] Department of Mechanical and Industrial Engineering, Ryerson University, 350 Victoria Street, Toronto, Ontario M5B 2K3, Canada
[b] Department of Mechanical and Mechatronics Engineering, University of Waterloo, 200 University Avenue West, Waterloo, Ontario N2L 3G1, Canada

ARTICLE INFO

Article history:
Received 31 May 2010
Received in revised form 24 August 2010
Accepted 25 August 2010
Available online 20 October 2010

Keywords:
Dual phase steel
Laser welding
Dissimilar welded joints
Microstructure
Tensile properties
Fatigue
Fractography

ABSTRACT

The use of dual phase (DP) steels in the automobile industry unavoidably involves welding and dynamic loading. The aim of this investigation was to evaluate the microstructural change and mechanical properties of laser welded dissimilar DP600/DP980 steel joints. The dissimilar joints showed a significant microstructural change from nearly full martensite in the fusion zone (FZ) to the unchanged ferrite–martensite dual-phase microstructure in the base metal. The welding resulted in a significant hardness increase in the FZ but the formation of a soft zone in the heat-affected zone (HAZ). The dissimilar welded joints were observed to exhibit a distinctive unsymmetrical hardness profile, yield-point-like phenomenon, and single-stage work hardening characteristic, with yield strength and work hardening rate lying in-between those of DP600 and DP980 base metals, and ultimate tensile strength equivalent to that of DP600 base metal. Although the welded joints showed a lower fatigue limit than the base metals, the fatigue life of the welded joints at higher stress amplitudes was almost the same as that of the DP600 base metal. The welded joints failed in the soft zone at the DP600 side under tensile loading and fatigue loading at the higher stress amplitudes. Fatigue crack initiation occurred from the specimen surface and crack propagation was characterized by typical fatigue striation together with secondary cracks.

1. Introduction

Due to recent legislations by governments that require the reduction in greenhouse gas emissions and fuel consumption to protect our precious environment and mitigate the recently realized man-made global warming and reduce costs as well, automotive industry is constantly seeking efficient methods to manufacture vehicles from lighter materials or the materials with higher strength and ductility so as to reduce the vehicle weight while guaranteeing improved occupant safety. The materials used for automotive applications must be easily formable, weldable, coatable, and repairable [1–3]. The unique combination of higher strength along with the larger elongation and higher work hardening rate [4,5] of dual-phase (DP) steel, compared to the steel grades of similar yield strength [6], gave it better acquiescence to the automobile manufacturer. DP steels normally contain dispersed islands of martensite in the ferrite matrix [5,7–13]. The ductility arises from ferrite while martensite accounts for the strength, and with increasing volume fraction of martensite the strength of the DP steels increases and the ductility decreases [12,14]. Usually ferrite–martensite DP steels are produced by intercritical annealing followed by rapid cooling [4,15]. During the intercritical annealing small pools of austenite are formed in the ferrite matrix, which subsequently transform into martensite upon rapid cooling. The austenite-to-martensite transformation, accompanied by a volume expansion, leads to mobile dislocations into the surrounding ferritic matrix. The mobility of these dislocations is responsible for the high initial work hardening rate and continuous deformation behavior in the DP steels [15,16]. The work hardening rate is also associated with the volume fraction of martensite which can be altered by manipulating the intercritical annealing temperatures [4].

It is sometimes stated that about half of a country's gross domestic product (GDP) is related to welding and joining in one way or another, and in the case of autobody structures welding is the most-widely used joining operation. Due to ease of automation and flexibility, laser welding has gained its popularity in metal joining industry and has been considered to replace potentially some other popular joining processes such as resistance spot welding [17] and friction stir welding [18,19]. The promising possibility of the laser welding has prompted the manufacturers to use it for both ferrous [20,21] and nonferrous [22,23] alloys.

Depending upon the application of structural materials the usage of dissimilar welding is of vital importance. In the case of dissimilar joining of nonferrous materials, microcracks [24] and intermetallics [19,24] were observed which played a key role in the crack initiation and propagation [19]. However, in the case

* Corresponding author. Tel.: +1 416 979 5000x6487; fax: +1 416 979 5265.
E-mail address: dchen@ryerson.ca (D.L. Chen).

0925-8388/$ – see front matter © 2010 Elsevier B.V. All rights reserved.
doi:10.1016/j.jallcom.2010.08.158

Nomenclature

σ	true stress
n	strain hardening
B	bainite
CP	crack propagation
EDS	energy dispersive X-ray spectroscopy
FZ	fusion zone
HAZ	heat effected zone
HSLA	high strength low alloy
M	martensite
SPF	sideplate ferrite
UTS	ultimate tensile strength
ε	true strain
K	strength coefficient
CI	crack initiation
DP	dual phase
F	ferrite
GDP	gross domestic product
HCF	high cycle fatigue
LCF	low cycle fatigue
SC	secondary crack
TM	tempered martensite
YS	yield strength

of dissimilar joining of ferrous materials no such crack formation has been reported and the mechanical properties of the welds were found to be dominated by the type of materials and welding parameters [25]. While a significant amount of work has been conducted on the mechanical properties of laser welded similar grades of DP steel joints [9,26,27], the mechanical properties of dissimilar grades of laser welded DP steel joints have not yet been reported. As an autobody involves steels having different strength levels, it is necessary to ascertain how the laser welding changes the microstructure and affects the mechanical properties in the dissimilar DP steel joints.

Previous studies on similar DP steel joints made with both laser welding [9,26,28–30] and spot welding [31] indicated that welding led to the occurrence of a soft zone in the heat-affected zone (HAZ) which was observed to be the consequence of the formation of tempered martensite (TM) in that area during welding, and the mechanical properties of the welded joints were significantly affected by the presence of soft zone [9,26,28–31]. Questions arose on if such a soft zone is still present; how the soft zone changes; and to what extent the soft zone affects the mechanical properties in the laser welded dissimilar DP steel joints. The present study was, therefore, aimed at evaluating the microstructural changes, tensile and fatigue properties with emphasis on the yielding characteristics and work hardening behavior of the laser welded dissimilar DP steel joints.

2. Experimental details

1.2 mm thick DP600 steel sheet with a galvannealed coating (46 g/m^2 at the top and 47 g/m^2 at the bottom) and 1.2 mm thick DP980 steel sheet with a galvannealed coating (60 g/m^2 at the top and 67 g/m^2 at the bottom) were selected in the present study. The chemical composition of the base metals is given in Table 1. The laser welding was done using a diode laser and the welding parameters used in the present study are shown in Table 2. The Nuvonyx ISL4000L diode laser head was mounted on a Panasonic VR6 robotic arm as shown in Fig. 1. The beam had a rectangular shape with a size of 12 mm × 0.9 mm at a focal length of 90 mm. Also, due to the power density of the diode laser it was restricted to conduction mode welding. During welding ultra-high purity argon was used as a shielding gas at a flow rate of 14.2 l/min.

Metallographic samples of the welded joints cut perpendicular to the welding direction were prepared and examined using light microscope and scanning electron microscope. Vickers microhardness was determined using a load of 500 g and a dwell time of 15 s. All the microhardness values presented in this study were an average of three series of values taken on the same specimen. The center point of the fusion zone was determined carefully after observing the weld geometry under microscope and all the indentations were adequately spaced to avoid any potential effect of strain field caused by adjacent indentations.

Tensile tests were performed using ASTM-E8M subsized samples on a fully computerized tensile testing machine at room temperature and strain rates from 1×10^{-5} to 1×10^{-2} s^{-1}. An extensometer with a gauge length of 25 mm was used to measure the strain during the test. The 0.2% offset yield strength, ultimate tensile strength, ductility and the work hardening properties were evaluated. Fatigue tests were performed on the same subsized samples on a fully computerized Instron 8801 servo-hydraulic testing system under load control at more than 6 stress amplitudes. The stress ratio of R equal to 0.1, sinusoidal waveform and a frequency of 50 Hz were selected in all the tests. The tensile and fatigue fracture surfaces were examined via JSM-6380 LV scanning electron microscope equipped with Oxford energy dispersive X-ray spectroscopy (EDS) system and 3D fractographic analysis.

Table 1
Chemical composition (wt%) of the dual phase steels selected in the present study.

Chemical composition	DP600	DP980
C	0.09	0.15
Mn	1.84	1.50
Si	0.36	0.31
Al	0.05	0.05
Mo	0.01	0.006
Cr	0.02	0.02
Cu	0.03	0.02
S	0.005	0.006
P	0.01	0.01

Table 2
Welding parameters selected in the present study.

Laser system	Nuvonyx ISL-4000
Laser source	Diode
Laser power (kW)	4
Welding speed (m/min)	1
Focal length (mm)	90
Beam dimension (mm^2)	12 × 0.9

3. Results and discussion

3.1. Microstructural evolution and microhardness profile

Fig. 2 shows SEM micrographs representing the typical microstructural changes occurred during the laser welding process. As seen from Fig. 2(a) the microstructure of DP600 base metal was characterized by martensite islands in the ferrite matrix. The HAZ microstructure at the DP600 side is shown in Fig. 2(b), consisting of tempered martensite (TM) and possibly bainite (B) along with some

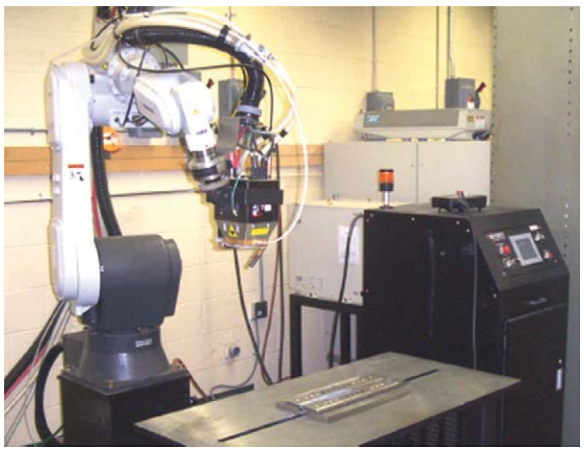

Fig. 1. The Nuvonyx ISL4000L diode laser head mounted on a Panasonic VR6 robotic arm.

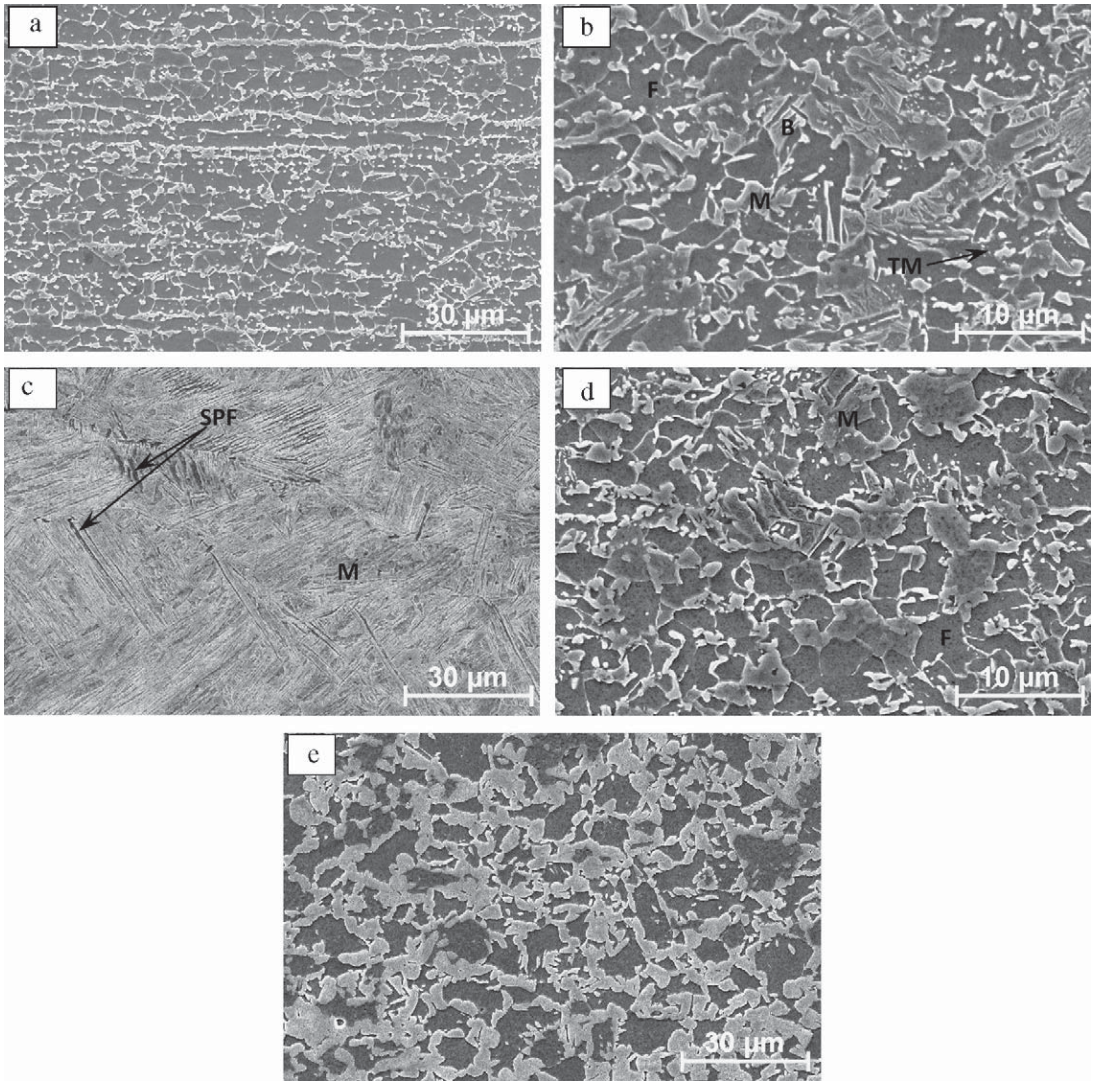

Fig. 2. SEM micrographs showing the microstructural change of a laser welded dissimilar dual-phase steel joint, (a) DP600 base metal, (b) HAZ (DP600), (c) fusion zone, (d) HAZ (DP980), (e) DP980 base metal (where M: martensite, TM: tempered martensite, B: Bainite, F: ferrite and SPF: sideplate ferrite).

preexisting martensite (M) in the ferrite (F) matrix. The fusion zone (FZ) of this kind of welded joints contained mainly martensite (M) along with sideplate ferrite (SPF) as seen from Fig. 2(c). The formation of martensite in the FZ was a result of the rapid cooling of the weld pool containing mixed DP600 and DP980 steels during the welding. At the other side of the FZ, the HAZ of DP980 steel showed the presence of tempered martensite along with some possible bainite in conjunction with some pre-existing martensite in the ferrite (F) matrix (Fig. 2(d)). Like DP600 steel, the DP980 base metal also contained martensite in the ferrite matrix, but with a higher volume fraction of martensite (Fig. 2(e)). The image analysis indicated that the volume fraction of martensite was 0.25 in the DP600 base metal and 0.52 in the DP980 base metal, respectively.

The microhardness profile of the laser welded dissimilar joint is shown in Fig. 3, corresponding directly to the microstructural change in Fig. 2. Significantly higher hardness in the FZ than that in both base metals was observed due to the formation of prevailing martensite (Fig. 2(c)). In the HAZ, there existed a significant hardness drop called "soft zone" as indicated in Fig. 3, in comparison with both the FZ and BM regions. The occurrence of the soft zone was partly attributed to the disappearance of martensite and partly due to tempering of the remaining martensite pre-existed in the base metals during laser welding. Similar observations have been reported in [9,26,30,32]. It is of interest to observe that the degree of softening was more severe and the size of the soft zone was larger at the DP980 side than at the DP600 side, exhibiting a

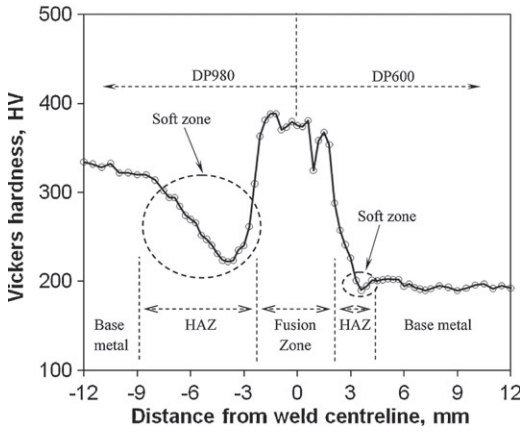

Fig. 3. A characteristic unsymmetrical microhardness profile of the laser welded DP600/DP980 dissimilar joint.

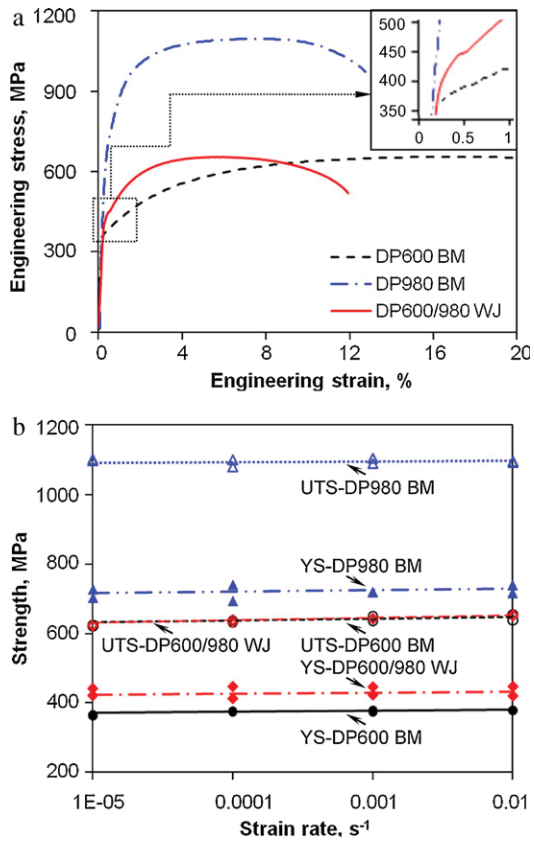

Fig. 4. (a) Typical stress–strain curves obtained at a strain rate of $1 \times 10^{-2}\ s^{-1}$, (b) effect of laser welding on the yield strength (YS) and ultimate tensile strength (UTS).

characteristic asymmetrical hardness profile across the dissimilar joint (Fig. 3). This was attributed to the vanishing and tempering of more pre-existing martensite at the DP980 side. It should be noted that although the degree of softening was more acute at the DP980 side, the lowest hardness value across the entire dissimilar joint was still positioned in the HAZ of DP600 side. The hardness in the base metals was nearly constant, and as expected DP980 base metal exhibited a higher hardness than DP600 base metal due to its higher volume fraction of martensite.

3.2. Tensile properties

Fig. 4(a) shows typical engineering stress–strain curves for both base metals and laser welded dissimilar DP joint tested at a strain rate of $1 \times 10^{-2}\ s^{-1}$. Although both base metals showed smooth and continuous stress–strain characteristics, the dissimilar welded joint exhibited a yield-point-like phenomenon which could be better seen from the inset of Fig. 4(a). Regarding the failure location all the dissimilar joints failed in the soft zone at the DP600 side, corresponding to the minimum hardness value in the microhardness profile across the dissimilar welded joint (Fig. 3). Careful observations during tensile tests showed that yielding started from the soft zone and the subsequent plastic deformation accumulated in this zone until final failure.

The presence of yield-point phenomena in the welded samples was likely due to interstitial diffusion which might occur during laser welding. The temperature generated in the welding process was high enough to drive the carbon or nitrogen atoms in iron to diffuse to the position of the high energy just below the extra plane of atoms in a positive edge dislocation. The strong elastic interaction alleviated the impurity atmosphere to become completely saturated and condense into a row of atoms along the core of the

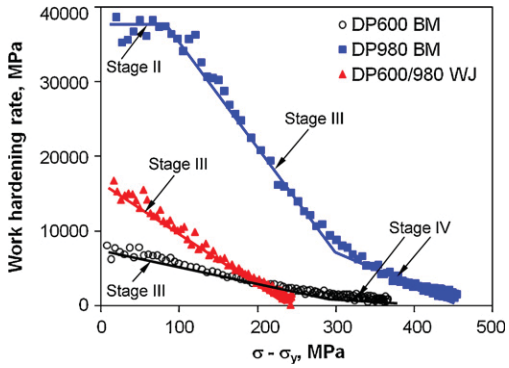

Fig. 5. Work hardening rate vs. net flow stress for the DP600 and DP980 base metals as well as DP600/DP980 dissimilar welded joints tested at a strain rate of $1 \times 10^{-2}\ s^{-1}$.

dislocation. When such a sample with dislocations pinned by interstitials (i.e., the welded samples in this study) was loaded, a higher stress was required to start the dislocation movement representing the onset of plastic deformation. Once the dislocation line was pulled free from the influence of the solute atoms, slip occurred at a lower stress, exhibiting a yield-point phenomenon [30,33,34].

While the yield-point-like phenomenon of the dissimilar welded joints was not so strong (Fig. 4(a)), the YS of the dissimilar welded joints was apparently higher than that of the DP600 base metal, as shown in Fig. 4(b). However, it was lower than the YS of DP980 base metal. The UTS of the dissimilar welded joints was observed to be essentially the same as that of the DP600 base metal. It is known that the UTS of a steel was proportional to its hardness value. While the welded joints showed softening at both sides of FZ, the degree of softening at the DP600 side was very small or insignificant (Fig. 3). Thus the UTS of the welded joints was almost identical to that of the DP600 base metal. In all cases both YS and UTS exhibited only a very weak strain rate dependence in the range between 1×10^{-5} and $1 \times 10^{-2}\ s^{-1}$. At higher strain rates the dislocation movement might be delayed, resulting in a slightly increased YS and UTS. It was also reported that the higher strain rate generated a dislocation morphology with more tangles in the cell walls and more refined cell size which in turn increased the strength [35]. Besides, it is seen from Fig. 4(a) that despite the higher YS and the same UTS, the dissimilar welded joint showed a lower ductility which was only equivalent to that of DP980 base metal but lower than that of DP600 base metal.

3.3. Work hardening characteristics

Fig. 5 presents a Kocks–Mecking type plot [36] of work hardening rate vs. net flow stress ($\sigma - \sigma_y$) at a strain rate of $1 \times 10^{-2}\ s^{-1}$. It is seen that the strain hardening rate of the dissimilar welded joint basically lay in-between those of DP600 and DP980 base metals. The welded joint and DP600 base metal showed basically stage III work hardening behavior as indicated by a linear decrease of work hardening rate with increasing flow stress (Fig. 5). While the dissimilar welded joints showed only stage III work hardening behavior, the DP600 base metal had stage IV work hardening behavior when the net flow stress exceeded approximately 270 MPa although the change of the value of work hardening rate was small. Unlike the dissimilar welded joint and DP600 base metal, the DP980 base metal displayed initially stage II work hardening behavior as indicated by almost constant work hardening rate up to a net flow stress of ~90 MPa (Fig. 5), followed by stage III hardening until ~300 MPa, and finally stage IV hardening appeared. The three stages of work hardening behavior could be described as follows: in stage II the constant work hardening rate was due to the deform-

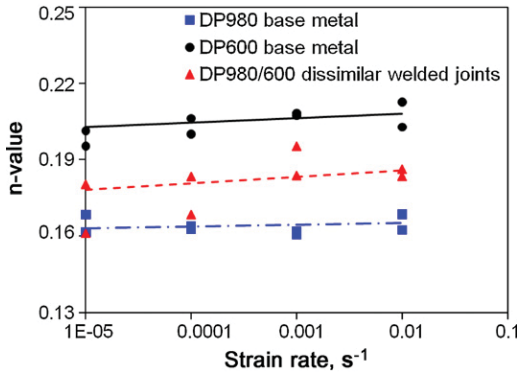

Fig. 6. Work hardening exponents at different strain rates evaluated using the Hollomon equation.

taion of constrained ferrite with possible transformation of retained autenite to martensite [37–39]. In stage III the linear decrease of work hardening rate arose from simultaneous deformation of ferrite and martensite with attendant cross-slip and dynamic recovery of ferrite [37–39]. In stage IV the low work hardening rate originated from increased dislocation mobility via profuse cross-slip [40].

After yielding the stress–strain relationship in the uniform deformation stage may be expressed by Hollomon equation [41],

$$\sigma = K\varepsilon^n, \quad (1)$$

where σ is the true stress, ε is the true strain, n is the strain hardening exponent and K is the strength coefficient. The evaluated n values following Eq. (1) as a function of strain rate are shown in Fig. 6. It is seen that DP600 steel possesed higher work hardening exponent than the DP980 steel, while the n value of the dissimilar welded joints lay in-between those of DP600 and DP980 base metals. This corresponded well to the results presented in Fig. 4(a). The work hardening exponent was also expected to be influenced by the volume fraction of martensite in the material. With increasing volume farction of martensite the value of n usually decreased [4]. It is believed that the work hardening in the DP steels was mainly associated with the amount of ferrite which was relatively soft in comparsion to martensite – the more the ferrite (or the less the volume farction of martensite), the higher the hardening capacity, since the capacity for the storage of dislocations and their interaction was higher. In all cases the values of n showed only a weak strain rate senitivity and incresed with increasing strain rate by a very small amount.

3.4. Fatigue properties

Fig. 7 depicts the obtained S–N curve for DP600/DP980 dissimilar joints. It is seen that at higher stress amplitudes the fatigue strength of the dissimilar welded joints was basically the same as that of DP600 base metal, which was however much lower than that of DP980 base metal. This was due to the fact that the DP980 base metal was much stronger as reflected by the considerably higher hardness (left-hand side in Fig. 3) and UTS (Fig. 4). The equivalent fatigue life or strength between the dissimilar welded joints and DP600 base metal suggested that the laser welding had little effect on the fatigue performance of DP600 steel at intermediate and higher stress amplitudes in spite of the occurrence of the soft zone. This could be understood via the result shown in Fig. 3, where the minimum hardness in the HAZ or soft zone at the DP600 side was only marginally lower than that the average hardness value of DP600 base metal. However, the welded joints showed a lower fatigue limit than the DP600 base metal (Fig. 7). This suggested

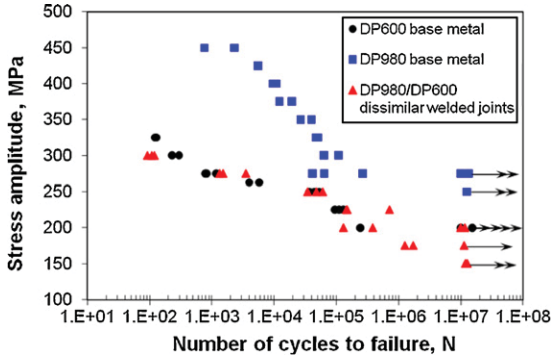

Fig. 7. S–N curves of the base metals and the dissimilar welded joints tested at $R = 0.1$, 50 Hz and room temperature where the run-out samples were indicated by arrow marks.

Table 3
Fatigue limit and fatigue ratio of the DP600 and DP980 base metals as well as DP600/DP980 dissimilar welded joints.

Material type	Fatigue limit (MPa)	Ultimate tensile strength (MPa)	Fatigue ratio
DP600 base metal	200	634	0.32
DP980 base metal	250	1095	0.23
DP600/980 dissimilar joints	150	638	0.24

that the slight reduction of the hardness in the soft zone did have an effect on the fatigue strength at lower stress amplitudes. The fatigue limit and the fatigue ratio of the materials tested in the present study are tabulated in Table 3. The fatigue limit of the dissimilar welded joints was observed to be lower than that of the DP600 and DP980 base metals by about 25% and 40%, respectively, whereas the obtained fatigue ratio of the dissimilar welded joints lay in-between the base metals but was close to that of DP980 base metal. The reduction of the fatigue limit insinuated that the HAZ softening of the weld played a significant role in the fatigue properties at lower stress amplitudes. Therefore, in the fatigue design and/or life prediction of the welded joints, it is necessary to take into account the weakening effect of welding on the fatigue limit so as to ensure the integrity and longevity of automotive components.

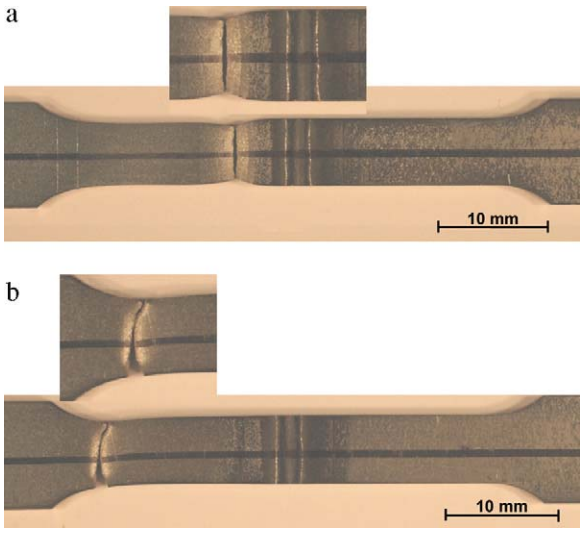

Fig. 8. Fatigue failure locations of the dissimilar welded joints tested at a stress amplitude of (a) 275 MPa, (b) 200 MPa.

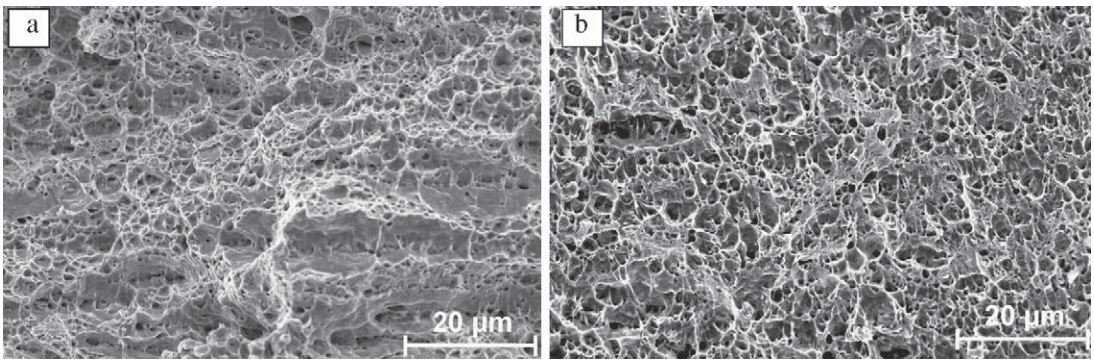

Fig. 9. Typical SEM micrographs of the tensile fracture surface of the welded joints tested at a strain rate of 1×10^{-2} s^{-1}, (a) in the specimen center and (b) near the specimen edge.

3.5. Fatigue failure location

While all the dissimilar welded joints failed exclusively in the soft zone at the DP600 side during tensile tests, the failure location of the welded joints was observed to be related to the applied stress amplitudes. The samples tested at lower stress amplitudes failed far away from the middle gauge section but the samples tested at higher stress amplitudes failed at the soft zone in the HAZ, as shown in Fig. 8. The possible reason for the occurrence of different failure locations would be explained by cyclic strengthening mech-

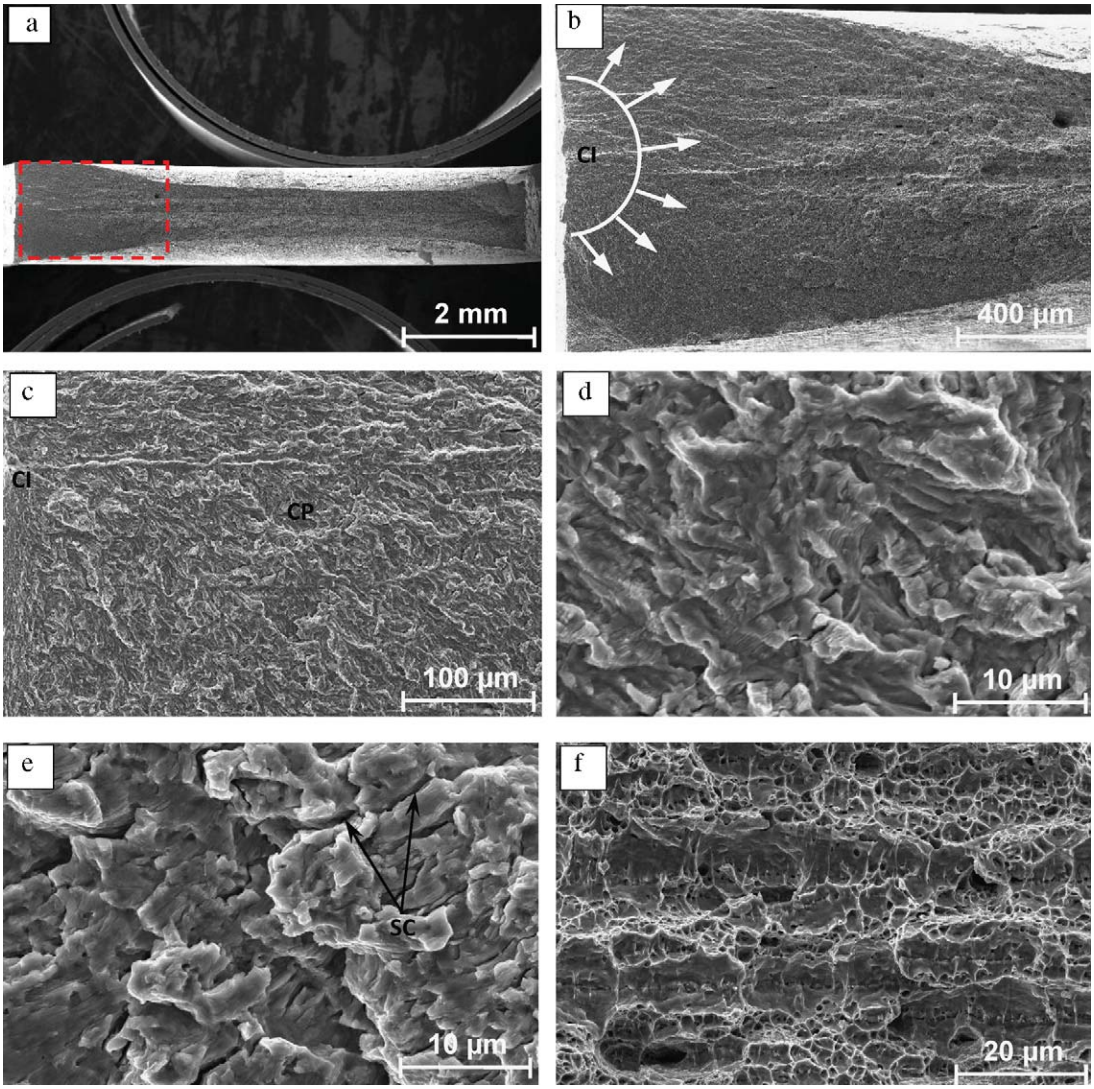

Fig. 10. Typical fatigue fracture surface of the welded joint tested at a stress amplitude of 225 MPa, (a) overall view of the fracture surface at a low magnification, (b) magnified view of the dashed box in (a) showing the crack initiation (CI) site, (c) crack propagation (CP) near the crack initiation site at an intermediate magnification, (d) crack propagation near the crack initiation site at a higher magnification, (e) crack propagation with secondary cracks (SC) at a higher magnification, (f) center of the fracture surface showing the final rapid crack propagation.

anism involving deformation-induced martensitic transformation [42–44]. Small amount of retained austenite contained in the DP steels could be transformed to martensite, giving rise to additional strengthening in the longer life high cycle fatigue (HCF) region. The newly formed martensite interacted with the dislocations [45] and made it tough at the relatively lower stress amplitudes to overcome the pinning force created by martensite. Then the area near the end of gauge section became the weakest due to the potential stress concentration caused by the notch effect. Indeed it has been pointed out that the notch effect was usually stronger in the longer life HCF region compared to the shorter life low cycle fatigue (LCF) region [46]. In the LCF region where the samples were tested at higher stress amplitudes the dislocations could more easily overcome the martensitic barriers as the magnitude of applied stress was high enough to cause more cumulative damage in the soft zone of the test samples. As a result, the welded dissimilar DP steels failed in the soft zone of DP600 side at higher stress amplitudes.

3.6. Fractography

The tensile fracture surface characteristics were basically similar in both the welded joints and DP600 base metal. The tensile fracture surfaces showed mostly equiaxed dimples (Fig. 9(a)) at the center indicating typical ductile fracture in the DP steels, regardless of the welding. The fracture surface near the specimen surface showed a combination of both equiaxed and elongated dimples near the edge (Fig. 9(b)), indicating the occurrence of shearing motion.

The fatigue samples tested at lower and intermediate stress amplitudes showed clearly the crack initiation site and crack propagation area on the fracture surface. A typical example of the overall fracture surface of a sample tested at 225 MPa is shown in Fig. 10(a). The crack initiation (CI) took place from the surface (Fig. 10(b)). The grains at the surface are normally less constrained than the interior grains so the occurrence of slip is easier near the surface during fatigue testing. These back and forth slip movement during fatigue testing can build up notches or ridges at the surface which are usually referred as extrusion and intrusion [33]. These kinds of notch with a notch root of atomic dimension acted as a stress raiser and might end up being the nucleation site of the fatigue crack. The surface roughness and protrusions could also act as a site of stress concentration which may lead to crack initiation during fatigue [28,30]. A magnified view of the crack initiation site is shown in Fig. 10(c), and the early stage of crack propagation (CP) near the crack initiation site is in Fig. 10(d), where fatigue striations could be seen but their spacing was very small, reflecting an initially slow rate of crack propagation. With increasing distance from the crack initiation site, the spacing of fatigue striations became gradually larger representing an increasingly faster propagation, as shown in (Fig. 10(e)). The fatigue striations occurred usually perpendicular to the propagation direction. The presence of secondary cracks (SC) was also evident in the faster crack propagation area, which appeared to increase with increasing distance from the initiation site as well. The formation of fatigue striations was basically considered to be due to a repeated plastic blunting–sharpening process caused by either dislocation slip [47] or twinning [48] in the plastic zone ahead of the fatigue crack tip. The final rapid crack propagation at the center of the fracture surface was mainly characterized by the cup-like dimples, as shown in Fig. 10(f), which was indeed the same as the monotonic tensile fracture surface characteristics (Fig. 9(a)). Both the base metals and the welded joints had similar fatigue fracture surface characteristics.

4. Conclusions

(a) The microstructural change across the dissimilar welded joints resulted in a significant hardness increase in the FZ (due to fully martensitic structure) but lower hardness values were observed in the HAZ. The degree of softening was more severe and the size of the soft zone was larger at the DP980 side than at the DP600 side, leading to a characteristic unsymmetrical hardness profile across the dissimilar welded joint.

(b) The dissimilar welded joints were observed to exhibit a yield-point-like phenomenon and only stage III work hardening behavior. The YS and work hardening rate of the dissimilar welded joints were higher than those of DP600 base metal but lower than those of DP980 base metal. The UTS of the dissimilar welded joints was essentially the same as that of the DP600 base metal while its ductility was equivalent to that of the DP980 base metal.

(c) The dissimilar welded joints exhibited a lower fatigue limit than the base metals, but at higher stress amplitudes they had almost the same fatigue life as DP600 base metal despite the presence of the soft zone.

(d) Under monotonic tensile loading all the dissimilar welded joints failed in the soft zone at the DP600 side and the fracture surfaces exhibited predominantly ductile type of fracture. The fatigue fracture location of the dissimilar welded joints was observed to be associated with the stress amplitude applied. While the fatigue failure occurred mainly in the soft zone at the higher stress amplitudes, nearly no failure appeared in the soft zone at the lower stress amplitudes due to the cyclic strengthening involving deformation-induced martensitic transformation. In all cases the fatigue fracture was observed to initiate from the specimen surface and the crack propagation was characterized by typical fatigue striation together with secondary cracks.

Acknowledgements

The authors would like to thank the Natural Sciences and Engineering Research Council of Canada (NSERC), and Initiative for Automotive Innovation (Ontario Research Fund – Research Excellence) for providing financial support. N.F. thanks Ryerson School of Graduate Studies for his SGS scholarship. D.L.C. is also grateful for the financial support by the Premier's Research Excellence Award (PREA), Canada Foundation for Innovation (CFI), and Ryerson Research Chair (RRC) program. The authors would like to thank J. Li (University of Waterloo), Q. Li, A. Machin, J. Amankrah, D. Ostrom, R. Churaman (Ryerson University) for their assistance in the experiments.

References

[1] M.S. Khan, S.D. Bhole, D.L. Chen, G. Boudreau, E. Biro, J. Van Deventer, Sci. Technol. Weld. Join. 14 (2009) 616–625.
[2] C. Ma, D.L. Chen, S.D. Bhole, G. Boudreau, A. Lee, E. Biro, Mater. Sci. Eng. A 485 (2008) 334–346.
[3] D. Anand, G. Boudreau, P. Andreychuk, D.L. Chen, S.D. Bhole, Can. Metall. Quart. 45 (2006) 189–198.
[4] P. Mohaved, S. Kolahgar, S.P.H. Marashi, M. Pouranvari, N. Parvin, Mater. Sci. Eng. A 518 (2009) 1–6.
[5] X. Zuo, Y. Chen, M. Wang, Y. Li, H. Wang, Z. Wang, Trans. Mater. Heat Treat. 31 (2010) 29–34.
[6] Advance High Strength Steel (AHSS) Application Guidelines, International Iron and Steel Institute, 2006, www.worldautosteel.com.
[7] Y.G. Ko, C.W. Lee, S. Namgung, D.H. Shin, J. Alloys Compd. 504 (2010) 452–455.
[8] A. Bahrami, S.H. Mousavi Anjidan, J. Alloys Compd. 392 (2005) 177–182.
[9] M. Xia, E. Biro, Z. Tian, Y.N. Zhou, ISIJ Int. 48 (2008) 809–814.
[10] S.R. Mediratta, V. Ramaswamy, V. Singh, P. Rama Rao, Trans. Indian Inst. Metals 38 (1985) 350–372.
[11] M. Pouranvari, S.P.H. Marashi, Sci. Technol. Weld. Join. 15 (2010) 149–155.
[12] D.L. Chen, Z.G. Wang, X.X. Jiang, S.H. Ai, C.H. Shih, Mater. Sci. Eng. A 108 (1989) 141–151.
[13] M.J. Molaei, A. Ekrami, Mater. Sci. Eng. A 527 (2009) 235–238.
[14] S. Kuang, Y. Kang, H. Yu, R. Liu, Int. J. Miner. Metall. Mater. 16 (2009) 159–164.
[15] R.G. Davies, Metall. Mater. Trans. A 10 (1979) 113–118.

[16] N.D. Beynon, S. Oliver, T.B. Jones, G. Fourlaris, Mater. Sci. Technol. 21 (2005) 771–778.
[17] X. Liao, X. Wang, Z. Guo, M. Wang, Y. Wu, Y. Rong, Mater. Charact. 61 (2010) 341–346.
[18] H. Shin, Y. Jung, J. Alloys Compd. 504 (2010) 279–282.
[19] A. Ambroziak, J. Alloys Compd. (2010), doi:10.1016/j.jallcom.2010.07.062.
[20] H.C. Lin, K.M. Lin, Y.C. Chuang, T.S. Chou, J. Alloys Compd. 306 (2000) 186–192.
[21] R.S. Sharma, P. Molian, Mater. Des. 30 (2009) 4146–4155.
[22] H.S. Wang, H.G. Chen, J.S.C. Jang, J. Alloys Compd. 495 (2010) 224–228.
[23] X.B. Liu, G. Yu, J. Guo, Y.J. Gu, M. Pang, C.Y. Zheng, H.H. Wang, J. Alloys Compd. 453 (2008) 371–378.
[24] T. Saeid, A. Abdollah-zadeh, B. Sazgari, J. Alloys Compd. 490 (2010) 652–655.
[25] E. Ahmed, U. Reisgen, M. Schleser, O. Mokrov, Sci. Technol. Weld. Join. 15 (2010) 337–342.
[26] M. Xia, N. Sreenivasan, S. Lawson, Y. Zhou, Z. Tian, J. Eng. Mater. 129 (2007) 446–452.
[27] C.Y. Kang, T.K. Han, B.K. Lee, J.K. Kim, Mater. Sci. Forum 539–543 (2007) 3967–3972.
[28] N. Farabi, D.L. Chen, Y. Zhou, Proc. Eng. 2 (2010) 835–843.
[29] S.K. Panda, M.L. Kuntz, Y. Zhou, Sci. Technol. Weld. Join. 14 (2009) 52–61.
[30] N. Farabi, D.L. Chen, J. Li, Y. Zhou, S.J. Dong, Mater. Sci. Eng. A 527 (2010) 1215–1222.
[31] V.H.B. Hernandez, S.K. Panda, Y. Okita, N.Y. Zhou, J. Mater. Sci. 45 (2010) 1638–1647.
[32] M.S. Xia, M.L. Kuntz, Z.L. Tian, Y. Zhou, Sci. Technol. Weld. Join. 13 (2008) 378–387.
[33] G.E. Dieter, Mechanical Metallurgy, SI Metric Edition, McGraw-Hill Book Co., UK, 1988.
[34] P. Movahed, S. Kolahgar, S.P.H. Marashi, M. Pouranvari, N. Parvin, Mater. Sci. Eng. A 518 (2009) 1–6.
[35] W.S. Lee, C. Lin, B. Chen, Proc. Inst. Mech. Eng. Part C 219 (2005) 439–451.
[36] U.F. Kocks, H. Mecking, Prog. Mater. Sci. 48 (2003) 171–273.
[37] T.S. Byun, I.S. Kim, J. Mater. Sci. 28 (1993) 2923–2932.
[38] A. Bag, K.K. Ray, E.S. Dwarakadasa, Metall. Mater. Trans. A 30 (1999) 1193–1202.
[39] S.N. Monteiro, R. Reed-Hill, Metall. Mater. Trans. B 2 (1971) 2947–2948.
[40] J. Cuddy, M. Nabil Bassim, Mater. Sci. Eng. A 113 (1989) 421–429.
[41] J.H. Hollomon, Am. Inst. Mining Metall. Eng. Trans.-Iron Steel Div. 162 (1945) 268–289.
[42] X. Cheng, R. Petrov, L. Zhao, M. Janssen, Eng. Fract. Mech. 75 (2008) 739–749.
[43] T.B. Hilditch, I.B. Timokhina, L.T. Robertson, E.V. Pereloma, P.D. Hodgson, Metall. Mater. Trans. A 40 (2009) 342–353.
[44] K. Sugimoto, M. Kobayashi, S. Yasuki, Metall. Mater. Trans. A 28 (1996) 2637–2644.
[45] P. Lukas, L. Kunz, Fract. Eng. Mater. Struct. 25 (2007) 747–753.
[46] M. Sauzay, P. Gilormini, Fatigue Fract. Eng. Mater. Struct. 23 (2000) 573–579.
[47] C. Laird, ASTM Spec. Tech. Publ. 415 (1967) 131–168.
[48] S. Begum, D.L. Chen, S. Xu, A.A. Luo, Metall. Mater. Trans. A 39 (2008) 3014–3026.